Journal of ELECTRONIC MATERIALS, Vol. 39, No. 6, 2010
DOI: 10.1007/s11664-010-1105-8
© 2010 TMS

Nucleation Mechanism of 6H-SiC Polytype Inclusions Inside 15R-SiC Crystals

YU ZHANG,[1] HUI CHEN,[1] GLORIA CHOI,[1]
BALAJI RAGHOTHAMACHAR,[1] MICHAEL DUDLEY,[1,5]
JAMES H. EDGAR,[2] KRZYSZTOF GRASZA,[3] EMIL TYMICKI,[3]
LIHUA ZHANG,[4] DONG SU,[4] and YIMEI ZHU[4]

1.—Department of Materials Science and Engineering, Stony Brook University, Stony Brook, NY, USA. 2.—Department of Chemical Engineering, Kansas State University, Manhattan, KS, USA. 3.—Institute of Electronic Materials Technology, Warsaw, Poland. 4.—Center for Functional Materials, Brookhaven National Laboratory, Upton, NY, USA. 5.—e-mail: mdudley@notes.cc.sunysb.edu

A model is presented for the nucleation mechanism of 6H-SiC polytype inclusions inside 15R-SiC boules. Inhomogeneous densities of screw dislocations lead to uneven growth rates, resulting in complex step overgrowth processes which can partially suppress the Burgers vector of a 15R 1c screw dislocation through the creation of Frank faults and Frank partial dislocations. Combined with stacking shifts induced by the passage of basal plane partial dislocations, it is shown that the partial Burgers vector suppression can leave behind a residual 6H 1c dislocation, which then acts as a nucleus for reproduction of 6H-SiC structure in the 15R-SiC crystal.

Key words: Polytype inclusion, polytype transformation, screw dislocation, partial dislocation

INTRODUCTION

Silicon carbide possesses outstanding properties such as high breakdown field, wide bandgap, high thermal conductivity, good chemical and mechanical stability, and high saturated electron drift velocity that constitute a significant improvement over conventional semiconductor materials for many envisaged applications. However, while some applications have already been realized, issues relating to crystalline defects and polytype inclusions remain a barrier to the successful realization of several others.

SiC is noted for its large number of polytypes.[1] Up to now, more than 200 types of phases of SiC have been found.[2,3] Due to the variety of polytypes and the limitation of growth condition control, it is fairly common to have polytype inclusions embedded in SiC crystals, which may lead to nucleation of device-killing micropipes.[4] Consequently, the nucleation mechanism of polytype inclusions in SiC crystals assumes great importance. The goal of this paper is to understand the nucleation mechanism of 6H-SiC polytype inclusions inside 15R-SiC crystals, so as to design strategies to mitigate their negative effects on SiC devices by completely eliminating them.

First, it is necessary to understand the stacking rules in SiC. The structure of SiC can be considered as an assembly of corner-sharing tetrahedra.[5–7] Every SiC tetrahedron arises from tetrahedral bonding between silicon and carbon atoms, and the SiC tetrahedra are joined to each other at their corners. A tetrahedron in a close-packed assembly of corner-sharing tetrahedra can occupy one of three sites on the *c*-plane: A, B, or C. By rotating the tetrahedron by 180° around the *c*-axis, we obtain a twinned tetrahedron with twinned variants A′, B′ or C′. The SiC polytypes consist of various stacking permutations of these six types of tetrahedra.

Corner-sharing places certain restrictions on the stacking of two tetrahedra on top of one another.[7]

(Received October 1, 2009; accepted January 29, 2010; published online February 24, 2010)

Therefore, we are able to obtain the stacking rules in SiC as: a tetrahedron should be followed by another one of the same variant or twinned variant but with the preceding letter, e.g., ABCA and A′C′B′A′, or AC′, BA′, CB′, A′B, B′C, and C′A. Based on the stacking rules in SiC, we can construct the stacking sequences of all types of SiC polytypes.

Pirouz and Yang[8] proposed a dislocation model for polytype transformation in SiC. The model is based on the asymmetry in the mobility of partial dislocations in SiC. According to the Frank–Read mechanism of dislocation multiplication, with one partial dislocation producing a fault as it moves and one partial dislocation almost immobile, a faulted loop is produced on the primary glide plane where the stacking sequence within the loop is changed. The dissociated screw dislocation cross-slips from the primary glide plane onto the next allowed slip plane according to the stacking rules. On every faulted glide plane, the tetrahedra transform to their twinned variants. Then, the dissociated screw dislocation double-cross-slips back onto the next allowed primary glide plane due to the compressive stress between the partial dislocations. The repeated glide by the leading partial dislocation followed by cross-slip of the screw dislocation thus leads to phase transformation in SiC. Based on this model, we are able to obtain similar mechanisms of polytype transformation from 4H-, 6H-, and 15R- to 3C-SiC (Fig. 1).

In this model, however, polytype transformation in SiC requires a significant difference in the mobility of Si- and C-core dislocations (a difference which only exists at temperatures significantly below the growth temperature), as well as the operation of a classic two-ended Frank-Reed source. In fact, x-ray topography (XRT) studies have shown that, close to the growth temperature, basal plane dislocations (BPDs) dissociate into partial dislocations which have similar mobility and move together in pairs. In addition, the slip of dislocations in noncubic polytypes of SiC is confined to the basal plane,[9] with the result that there is no cross-slip. Regarding the operation of two-ended Frank-Read sources, the general absence of cross-slip makes it difficult to isolate a segment of BPD pinned at two points. Threading edge dislocations can act as pinning points but they are ineffective at pinning moving BPDs. Threading screw dislocations (TSDs) can also pin BPDs, as well as lock them into position in such a way that the activation of the Frank–Read source is prevented.[10] In this case, we need a new model to explain the nucleation mechanism for polytype transformation in SiC.

EXPERIMENTAL PROCEDURES

On axis, *a*-plane 15R-SiC crystals with 6H-SiC polytype inclusions were studied using nondestructive synchrotron white-beam x-ray topography (SWBXT) at the Stony Brook topography station at the National Synchrotron Light Source, Brookhaven National Laboratory and using monochromatic XRT at the Advanced Photon Source, Argon National Laboratory. Global views of the quality and structure of the crystals were initially obtained by recording transmission Laue patterns from the whole crystal volume. This was achieved by scanning the crystal and the film in the path of a slit-collimated beam. This enabled the polytype distribution to be determined as well as the distribution of defects and overall crystal quality. Based on the results of these global studies, areas of interest were identified, which were then investigated in detail in various diffraction geometries. Following this, in-plane transmission electron

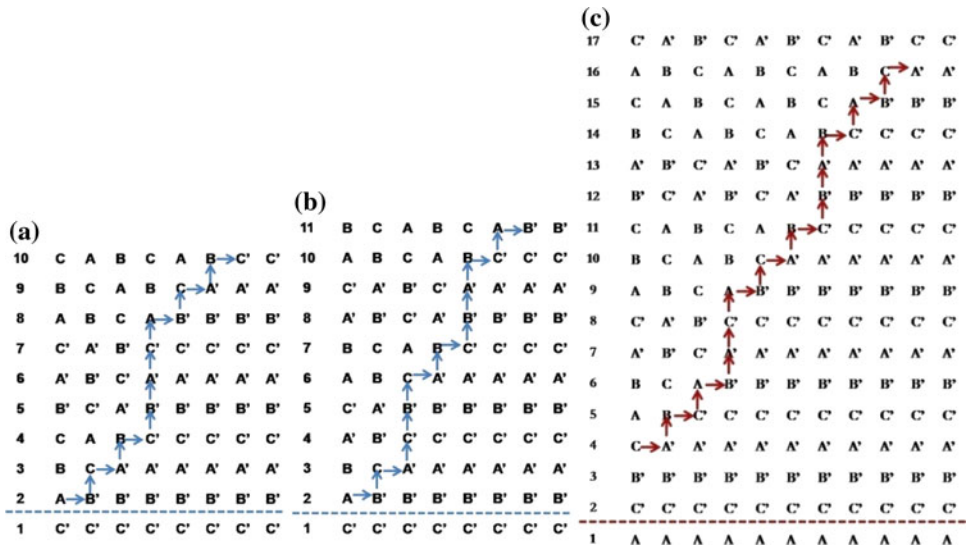

Fig. 1. Change in the stacking sequences from 6H- (a), 4H- (b), and 15R-SiC (c) to 3C-SiC during polytype transformation by the sequential formation of a faulted loop on the basal plane and cross-slip of screw dislocation to the next allowed basal plane.

microscope (TEM) specimens from the transition regions between 15R- and 6H-SiC were prepared parallel to $(11\bar{2}0)_{15R-SiC}$. High-resolution TEM (HRTEM) observation was performed using a JEOL 2100 TEM with an electron accelerating voltage of 200 keV.

RESULTS AND DISCUSSION

From scanning SWBXT results (Fig. 2a and b), we were able to distinguish diffraction patterns from both 6H- and 15R-SiC, as the large-area diffraction spots indicated by red upper-case letters can be indexed using the 15R structure, and diffraction spots indicated by orange lower-case letters correspond to the 6H structure.

Figure 2c–f shows details of 000·15 monochromatic transmission x-ray topographs recorded from both of the samples and enlarged images from the polytype regions. Since the basal planes of both the 15R and 6H regions are parallel, no orientation contrast is visible for this reflection. i.e., the 15R and 6H regions appear side by side. However, due to slight differences in bilayer spacing between the 15R and 6H polytypes, strain contrast, appearing as a dark line, is visible at the interface between the two regions. Long linear features are also visible running approximately parallel to the [0001] growth axis, which appear to be TSDs from their contrast. This shows that the number of dislocations terminating on the lower side of the inclusion is not the same as the number emanating from the top side of the inclusion back into the 15R region.

Based on the growth dislocation nature of TSDs present in the samples and the unequal number of TSDs at both sides of the polytype inclusion, we can draw the conclusion that the 6H-SiC polytype inclusions are generated during growth. Compared with this case, if polytype inclusions are generated after growth, densities of screw dislocations on each side of the 6H-SiC polytype inclusion should be the same as dictated by Burgers vector conservation.

According to the fact that 6H-SiC polytype inclusions are generated during growth, we need to consider the step-flow growth process in SiC. In this type of growth, spiral steps on the surface of SiC act

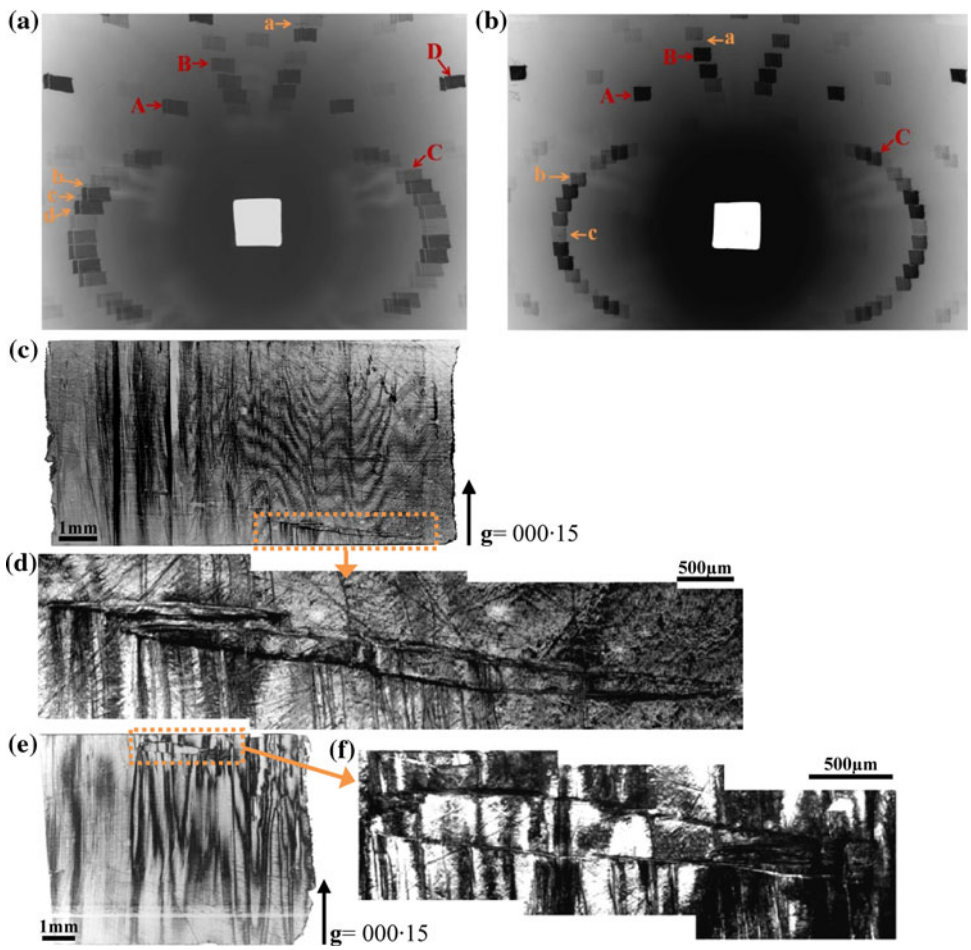

Fig. 2. (a, b) Scanning transmission SWBXT images of 15R-SiC substrates with 6H-SiC inclusions. Red upper-case letters indicate the diffraction spots from 15R-SiC. Orange lower-case letters indicate the diffraction spots from 6H-SiC inclusion. (c–f) Monochromatic 000·15 transmission x-ray topograph of two samples showing the detailed information around polytype inclusion region.

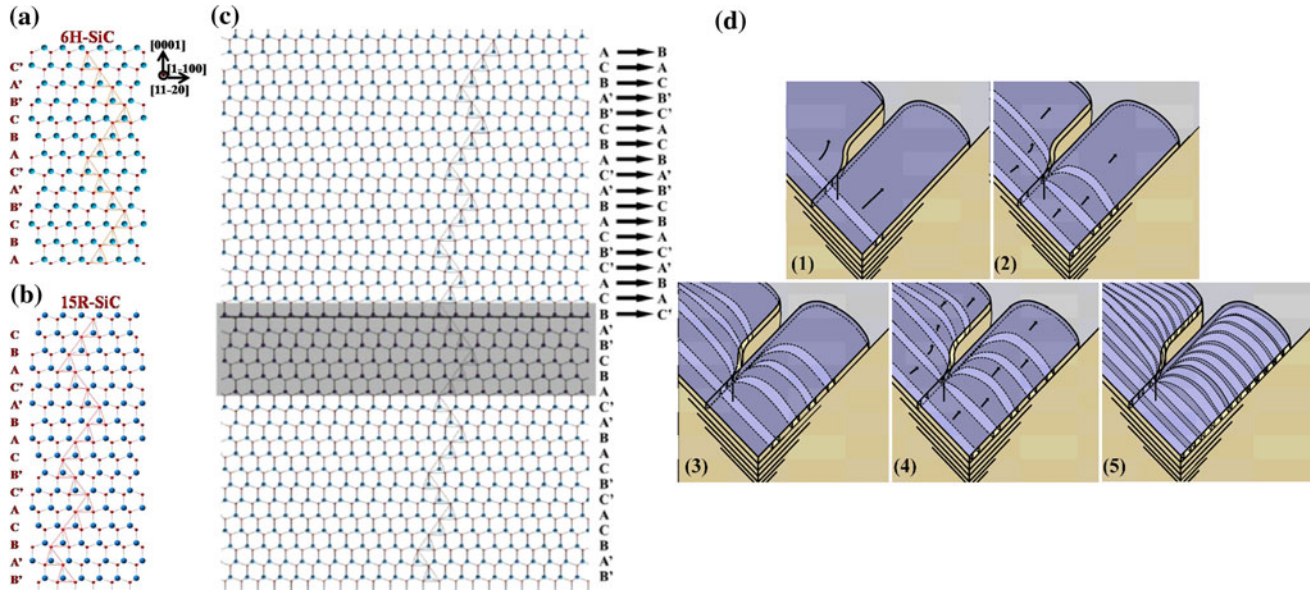

Fig. 3. Stacking sequences of 6H-SiC (a), 15R-SiC (b), and the model of polytype transformation from 6H to 15R (c). (d) Schematic diagrams of the interference between screw dislocation and basal plane partial dislocations.

as growth nucleation sites with active dangling bonds facing outwards on the step riser and thus will start to wind up around the dislocation core into growth spirals. Therefore the growth front will reproduce the structure of spiral steps as the crystal continues to grow. All steps which contain more than one bilayer can split into several energy-favorable, smaller step risers.

Comparing the stacking sequence of 6H- and 15R-SiC (Fig. 3a and b), we can establish a model for polytype transformation from 6H to 15R with the passage of a Shockley partial dislocation through the 15R structure (Fig. 3c) on the bold slip plane, creating a small volume of 6H structure. This small, isolated volume emerges as a nucleus of 6H structure during the step-flow process around a 1c screw dislocation in 15R-SiC. It is also necessary to consider how the screw dislocations interfere with basal plane partial dislocations during growth (Fig. 3d). The faulted region between two partial dislocations (lighter blue region) gets pinned by the screw dislocation core as the crystal grows. More and more faults pass the dislocation core, pile up, and form a larger faulted region around the screw dislocation core within which the stacking sequences are changed.

In step-flow growth of 15R-SiC, with the absence of a basal plane partial dislocation, terraces labeled with arrows (Fig. 4a) can continue to be overgrown by the vicinal step while the other ones cannot according to the stacking rules. This process will lead to the split of vicinal steps at the dislocation core, step bunching, and reproduction of the 1c 15R screw dislocation around the dislocation core.

Figure 4b shows step-flow growth in 15R-SiC with the passage of a partial dislocation resulting in the change of stacking sequences. More terraces with arrows can now continue to be overgrown by the vicinal step according to the stacking rules. Of the 1c 15R screw dislocation Burgers vector, 9/15 is suppressed by overgrowth of the advancing vicinal step, thereby converting parts of the TSD Burgers vector into Frank partial dislocations spanned by associated Frank [11] and leaving in the wake of the advancing step a small 6H-SiC nucleus. The 6H-SiC structure is then reproduced and forms the 6H-SiC inclusion.

The sample was then studied using HRTEM. Figure 5a shows the HRTEM image obtained from a pure 6H-SiC region using the $[11\bar{2}0]$ beam direction. Compared with the simulated atomic model with the same viewing direction (Fig. 5b), it can be seen that pairs of Si-C atoms appear as a single bright spot in the image. Three neighboring bright spots correspond to one tetrahedron with untwinned or twinned orientation. Three untwinned and three twinned tetrahedra form the structure of 6H-SiC and the stacking sequence of ABCB′A′C′. A selected-area diffraction (SAD) pattern of 6H-SiC was also obtained from the same region (Fig. 5c), matching perfectly with the simulated diffraction pattern (Fig. 5d).

An HRTEM image was also obtained from the pure 15R-SiC region for the $[11\bar{2}0]$ zone axis (Fig. 5e). The bright contrast comes from electron diffraction by Si-C clusters (Fig. 5f). Two untwinned tetrahedra are followed by three twinned tetrahedra that form the 15R-SiC structure and the stacking sequence of B′A′BCAC′B′CABA′C′ABC. The SAD pattern from pure 15R-SiC region (Fig. 5g) matches the simulated diffraction pattern (Fig. 5h).

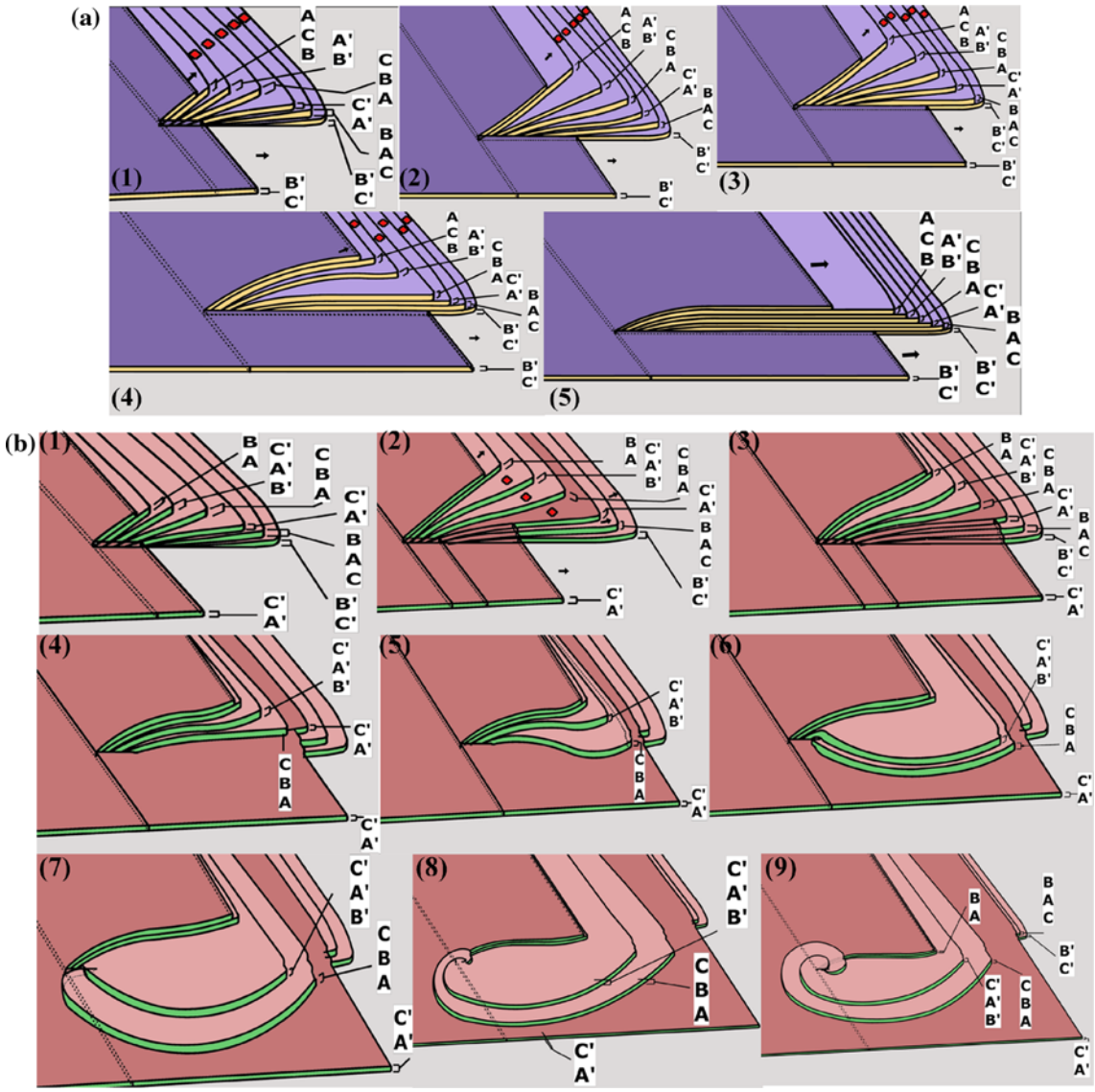

Fig. 4. (a) Schematic diagrams of step-flow growth in 15R-SiC without the passage of partial dislocation; (b) schematic diagrams of step-flow growth in 15R-SiC with the passage of partial dislocation.

We were able to locate the transition region between 15R- and 6H-SiC in the specimen based on the change in SAD pattern. Figure 5i shows the HRTEM image taken from the mixed region. Within the HRTEM image is what appears to be a 1c 6H screw dislocation (Fig. 5l), corresponding to a schematic diagram of a screw dislocation within 6H-SiC (Fig. 5j). Furthermore, there is evidence for the presence of Frank faults and partial dislocations within the center of the HRTEM image, manifested as extra atomic planes. An SAD pattern was also obtained from the same region (Fig. 5k), indicating diffraction patterns from both 6H- and 15R-SiC. Regular green arrows point to the five diffraction spots from 6H-SiC and red bold ones point to two spots from 15R-SiC. The remaining two spots overlap with those from 6H-SiC.

CONCLUSIONS

A new model is presented for the nucleation mechanism of 6H-SiC polytype inclusions in 15R-SiC boules grown by physical vapor transport. Inhomogeneous densities of screw dislocations replicated from the seed lead to uneven growth rates in the boule, resulting in a quasivicinal growth surface. Subsequent interference between advancing vicinal growth steps and screw dislocation spiral growth steps leads to complex step overgrowth processes which can suppress all or part of the 15R 1c screw dislocation Burgers vector through the creation of Frank faults and Frank partial dislocations on the basal plane. Combined with stacking shifts induced by the passage of basal plane partial dislocations, it is shown that suppression of 9/15 of

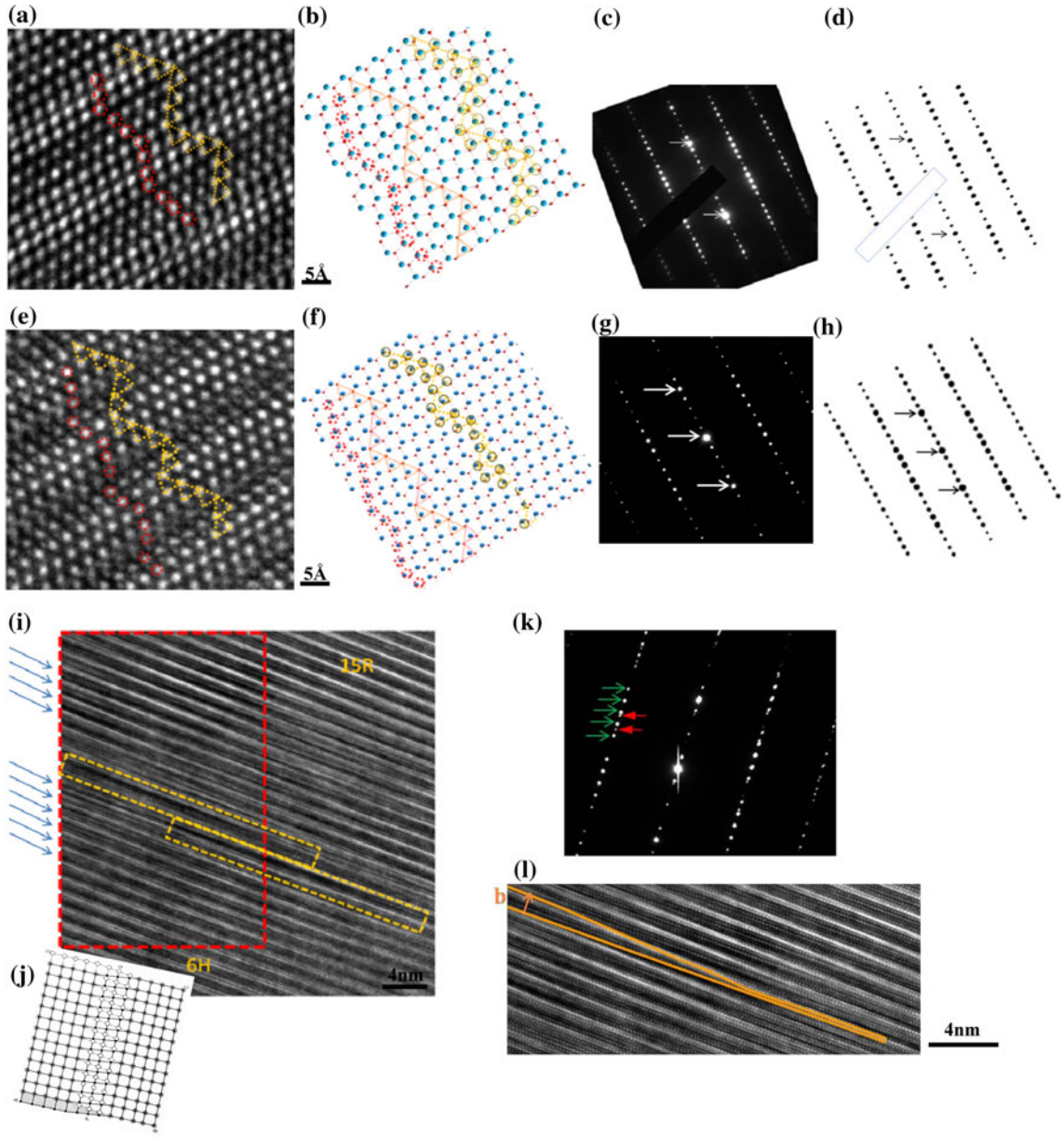

Fig. 5. (a) HRTEM image of pure 6H-SiC region; (b) simulated atomic model of 6H-SiC structure; (c) SAD pattern from the pure 6H-SiC region; (d) simulated diffraction pattern of 6H-SiC; (e) HRTEM image of pure 15H-SiC region; (f) simulated atomic model of 15H-SiC structure; (g) SAD pattern from the pure 15H-SiC region; (h) simulated diffraction pattern of 15H-SiC; (i) HRTEM image recorded from the transitional layer between 15R- and 6H-SiC; (j) schematic diagram of screw dislocation; (k) SAD pattern from the mixed region; (l) enlarged HRTEM image showing 1c 6H screw dislocation.

the 15R 1c dislocation Burgers vector by such step overgrowth can leave behind a residual Burgers vector corresponding to a 1c dislocation in 6H-SiC. The residual dislocation then acts as a nucleus for reproduction of the 6H-SiC structure at the surface of the 15R-SiC crystal.

REFERENCES

1. H. Baumhauer, *Z. Kristallogr.* 50, 33 (1912).
2. W. Shockley, *Silicon Carbide: A High Temperature Semiconductor*, ed. J.R. O'Connor and J. Smiltens (Oxford: Pergamon, 1960), .
3. P. Krishna, ed., *Progress in Crystal Growth and Characterization*, Vol. 7 (Oxford: Pergamon, 1983) and references therein.
4. M. Dudley, X.R. Huang, W. Huang, A. Powell, S. Wang, P. Neudeck, and M. Skowronski, *Appl. Phys. Lett.* 75, 784–786 (1999).
5. A. Verma and P. Krishna, *Polymorphism and Polytypism in Crystals* (New York: Wiley, 1966).
6. N.W. Jepps and T. Page, *Progress in Crystal Growth and Characterization*, Vol. 7, ed. P. Krishna (Oxford: Pergamon, 1983), pp. 259–306.
7. J.A. Powell, P. Pirouz, and W.J. Choyke, *Semiconductor Interfaces, Microstructure and Devices: Properties and Applications*, ed. Z.C. Feng (Bristol: Hilger, 1992).
8. P. Pirouz and J.W. Yang, *Ultramicroscopy* 51, 189–214 (1993).
9. P. Pirouz, M. Zhang, J.L. Dement, and H.M. Hobgood, *J. Appl. Phys.* 93, 3279 (2003).
10. Y. Chen, G. Dhanaraj, W. Vetter, R. Ma, and M. Dudley, *Mater. Sci. Forum* 556–557, 231 (2007).